RSC Advances

Transport properties of APdCu(Se2)(Se3) (A= K and Rb): New quaternary copper palladium polyselenides

Journal:	*RSC Advances*
Manuscript ID:	RA-ART-03-2014-002465.R1
Article Type:	Paper
Date Submitted by the Author:	02-Apr-2014
Complete List of Authors:	Azam, S; New Technologies - Research Center, University of West Bohemia, Univerzitni , Mechanical Engineering Reshak, A; New Technologies - Research Center, University of West Bohemia,, Mechanical Engineering

Transport properties of $APdCu(Se_2)(Se_3)$ (A= K and Rb): New quaternary copper palladium polyselenides

Sikander Azam*[1], A. H. Reshak[1,2],

[1] *New Technologies - Research Centre, University of West Bohemia, Univerzitni 8, 306 14 Pilsen, Czech republic*

[2] *Center of Excellence Geopolymer and Green Technology, School of Material Engineering, University Malaysia Perlis, 01007 Kangar, Perlis, Malaysia*

Abstract:

The electronic structure, effective mass, optical properties and electrical transport coefficients of $APdCu(Se_2)(Se_3)$ (A= K and Rb) a new quaternary copper palladium poly selenides have been investigated by density functional theory calculation within GGA+U approximation. The electronic band structure show that the calculated compounds possess direct band gap. From the partial density of states (PDOS) we found that, at energy -5.0 eV, Pd-s state strongly hybridize with Se-p state, near Fermi level the Se-p state hybridize with Cu-p state, and at the lower conduction band the Pd-s state form strong hybridization with Cu-s state. The investigation of electronic charge density shows that Pd-Se and Cu-Se atoms forms weak covalent bonding and strong iconicity, while K/Pd atoms exhibit pure ionic bonding. We also have calculated the dielectric function, refractive index, extinction coefficient, absorption coefficient, and the reflectivity. The calculated transport coefficients exhibit the anisotropic nature, in agreement with its electronic states. The transport properties reveal the stronger carrier transport along the Cu–p/d and Pd–d orbitals, indicating these orbitals are mainly responsible for electrical transport. The maximum power factor values of $KPdCu(Se_2)(Se_3)$ ($RbPdCu(Se_2)(Se_3)$) compounds as a function of relaxation time reach to 2.2 (1.8)$\times 10^{11}$, 4.4 (3.5) $\times 10^{11}$ and 1.3 (1.4) $\times 10^{11}$ within P^{xx}, P^{yy} and P^{zz} components, respectively.

Keywords: Band structure, TDOS and PDOS, Transport properties: DFT

*Corresponding author: Sikander Azam

Email: sikander.physicst@gmail.com

1. Introduction

Chalcogenides holds the most diverse and motivating structural chemistry, and display useful physical and chemical properties which are capable for applications in modern technologies [1]. The syntheses of binary and ternary chalcogenides have been broadly studied by most of the researchers in recent time. Using high-temperature solid state, intermediate-temperature flux, and low-temperature solvothermal techniques, but comparatively much little is known about quaternary chalcogenides

which may also demonstrate interesting properties [2-5]. In recent study the syntheses of novel quaternary chalcogenides are becoming an active area of solid state chemistry [2,4,5]. Till now the most known quaternary chalcogenides are made using the molten alkali-metal polychalcogenide flux technique; though, low-temperature solvo (hydro) thermal reactions have created a limited number of quaternary chalcogenides [6].

The Pd-holding compounds have got much consideration due to the catalytic functions of the metal and its capability to form poly chalcogenide complexes in solution media. In last years, a numeral ternary Pd poly chalcogenides have been isolated and structurally characterized. These encompass $(Ph_4P)_2[Pd(Se_4)_2]$ with distinct $[Pd(Se_4)_2]^{2-}$ anions in which each Pd^{2+} is coordinated by two chelating $(Se_4)^{2-}$ ligands [7] $\{(CH_3)N(CH_2CH_2)_3N\}_2[Pd(Se_6)_2]$ and $(enH)_2[Pd(Se_5)_2]$ featuring sheet-like, two-dimensional (2D) Pd polyselenide anionic frameworks [8] $Rb_2[Pd(Se_4)_2]Se_8$ encompassing sheet-like polyanion $[Pd(Se_4)_2]^{2-}$ with "intercalated" crown-like Se_8 eight-membered rings [9] and K4[Pd(Se4)2][Pd(Se$_6$)$_2$] (=K_2PdSe_{10}) and $Cs_2[Pd(Se_4)_2]$ (=Cs_2PdSe_8) having three dimensional (3D) structures assembled from two interpenetrating $[Pd(Sex)_2]^{2-}$ structures (x= 4 and 6 for the K^+ saline, x= 4 and 4 for the Cs^+ salt) [10,11].

In the system of A-M-M□-Q (A = alkali steel, M = assembly I element, M□= assembly VIII steel, Q = chalcogen), only some Fe compounds with the crystal formula of $AMFeQ_2$ (A = Li, Na, K, and Cs; M = Cu, Ag; Q = S, Se, Te) are knowned [12-16]. In 2003 Chen et al. [17] reported the groundwork, crystal organizations, and optical and thermal properties of two innovative mixtures, $APdCu(Se_2)(Se_3)$ (A = K and Rb), which are the first quaternary copper palladium poly chalcogenides obtained by solvothermal procedures utilizing ethylenediamine (en) as a reaction medium.

The target of the present study is the valuation of $APdCu(Se_2)(Se_3)$ (A= K and Rb). We calculated the thermoelectric properties, in the literature there is no study on these compound regarding such study.

In this paper, we aim at providing a systematic study of the electronic band structure, optical and thermoelectric properties of $APdCu(Se_2)(Se_3)$ (A= K and Rb) using DFT + U calculations. The GGA+U exchange potential approximation was used to calculate accurately the electronic band structure, optical and thermoelectric properties of $APdCu(Se_2)(Se_3)$ (A= K and Rb). As DFT+U scheme for solids have been shown to actually give better band gaps than semilocal DFT methods [18,19]

The optical properties help us to get deep insight into the structure of the $APdCu(Se_2)(Se_3)$ (A= K and Rb). The electrical transport parameters (conductivity, Seebeck coefficient, power factor) for the compound system are obtained theoretically based on the DFT calculation results and the rigid band approach.

The rest of the paper has been divided in four parts. In Section 2, we briefly describe the computational method used in this study. The most relevant results obtained for the electronic, optical and the thermo-electric properties of $APdCu(Se_2)(Se_3)$ (A= K and Rb) are presented and discussed in Section 3. Finally, we summarize the main conclusions in Section 4.

2. Methodology

It was recently reported that the local density approximation (LDA) and generalized gradient approximations (GGA) schemes are not sufficient to describe the electronic structure correctly for transition metal oxides [20].

Therefore, the GGA + U method was applied here to account for on-site correlation at the transition metal sites. The GGA + U method accounts for an orbital dependence of the Coulomb-exchange interaction was used for the present calculations. The crystal structure of new quaternary copper palladium polyselenides with monoclinic symmetry has been determined by Chen et al. [17]. The unit cell with formula $APdCu(Se_2)(Se_3)$ (A= K and Rb) was modeled for the pure phase property calculation simulations, i.e. electronic states and transport parameters calculation. The unit cell crystal structures for both compounds is illustrated in Fig. 1. Calculations with the full potential linear augmented plane wave method based on the DFT [21,22] theory were performed using Wien2k Package [23]. Exchange and correlation was computed within GGA+U [24]

The ground state properties of the resulting optimized structures have then been computed by performing self-consistent interactions until the iterative convergence of energy and charge to a value less than 10^{-5} Ry and 10^{-4} coulomb, respectively. We have calculated the bonds lengths and angles which shows good agreement with the experimental data [17] as shown in Table 1 and 2. We have used the parameter $R_{MT}K_{MAX}=7$ (where R_{MT} is the smallest of the muffin-tin radii and K_{MAX} is the plane wave cut-off) to control the size of basis set for the wave functions. The electronic band structure, total and partial density of states and the linear optical susceptibilities were calculated using summation over 1000 **k**-points within the IBZ. The Monkhorst-pack grid 11×10×8 was used for k-point sampling in the

electronic state calculation. The high symmetry **k**-points in the Brillouin zone (BZ) within our calculated band structure are Z→B→G→Y→G→Z. To initiate the calculations we have used the experimental values for lattice parameter taken from ref.17. The atomic positions are fully optimized by minimizing the forces acting of each atom. The optical properties of matter can be described by means of the dielectric function $\varepsilon(\omega)$. In the limit of linear optics, neglecting electron polarization effects and within the frame of random phase approximation the expression for the imaginary part $\varepsilon_2(\omega)$ of the dielectric function is calculated from the momentum matrix elements between the occupied and unoccupied wave functions. The real part $\varepsilon_1(\omega)$ of dielectric function is evaluated from imaginary part $\varepsilon_2(\omega)$ by the Kramers-Kroning transformation. The other optical constants, such as the reflective index, extinction coefficient, reflectivity and energy-loss spectrum can be obtained from $\varepsilon_1(\omega)$ and $\varepsilon_2(\omega)$.

The electrical transport coefficients were calculated with in the framework of semiclassical Boltzmann theory and the rigid band approach by analyzing the band structure from DFT calculations [25,26]. The transport distribution function to conductivity with in the rigid band approach is based on the following tensor:

$$\sigma_{\alpha\beta}(\varepsilon) = \frac{1}{N}\sum_{i,k}\sigma_{\alpha\beta}(i,k)(\varepsilon - \varepsilon_{i,k}) \quad \text{.....(1)}$$

where 1/N accounts for the normalization of the sum so it is the integral in the limit where the number of grid points becomes dense, $\varepsilon_{i,k}$ is the electron band energy for band i at Brillouin **k** point, the $\sigma_{\alpha\beta}(i,k)$ is the k-dependent conductivity tensor expressed as

$$\sigma_{\alpha\beta}(i,k) = e^2\upsilon_\alpha(i,k)\upsilon_\beta(i,k)\tau \quad \text{.....(2)}$$

where the $\upsilon_\alpha(i,k), \upsilon_\beta(i,k), \tau_e$ are the components of the band velocities and the relaxation time, respectively. In the band velocity expression $\upsilon_\alpha(i,k)$ the i denotes the bands, the k denotes the wave vector and the α denotes the direction. Afterward the transport coefficients can be deliberated by integrating the tensor within Eq. (1) as a function of temperature as

$$\sigma_{\alpha\beta}(T,\mu) = \frac{1}{\Omega}\int\sigma_{\alpha\beta}(\varepsilon)\left[-\frac{\partial f_\mu(T,E)}{\partial\varepsilon}\right]d\varepsilon \quad \text{.....(3)}$$

where the f comprises the Fermi distribution function, the T is the absolute temperature, the μ is the chemical potential and Ω is the volume. In the rigid band approach, the bands and $\sigma(\varepsilon)$ held fixed, as a

result only one band structure assessment is required to be executed [27]. The amount of carriers can be altered by varying the chemical potential μ. The purposes can thereafter be calculated from the band structure outcomes except for the relaxation time. Theoretically, the relaxation time period is correlated with crystal structure, temperature as well doping content, microstructure and texture of specific materials [28].

In general, the τ_e is resolute by the ratio of carrier energy $\varepsilon_{i,k}$ and the attained vibrational energy of atoms. The carrier power $\varepsilon_{i,k}$ is reliant on power catalogue i and wave vector k, the attained vibrational power of atoms is in the order of magnitude of $K_\beta T$. Much research is need analytically elucidate the scattering means and figure out the approximate valve of τ_e for specific materials. Regardless, the relaxation time τ_e has been broadly measured as a constant, and the carrier scattering is indulgenced as independent on vector direction and temperature for approximation of the real scattering means inside numerous works for calculation convenience [29,30].

With the constant relaxation time approximation, the Seebeck coefficient can be devised by

$$\alpha = \pm\frac{1}{eT}\left[E_F - \int_0^\infty g(E)\tau_e E^2 \frac{df_0(E)}{dE} \Big/ \int_0^\infty g(E)\tau_e E \frac{df_0(E)}{dE}\right] \text{..... (4)}$$

where the e, E_F, g(E), τ_e are the charge of the electron, Fermi level, density of state and relaxation time, respectively [31]. The Fermi level (E_F) and the density of state g(E) as a function of E can be obtained from the DFT computed results, the relaxation time τ_e is treated roughly as an unchanging, thus the Seebeck coefficient as a function of temperature T can be resolute. The BoltzTraP program was utilized for assessment of the k-dependent conductivity tensor. The BoltzTraP relies on a well checked smoothed Fourier interpolation to get an analytical sign of the bands [32]. The initial k mesh was interpolated up on a mesh five times denser than the original.

3. Results and discussion

3.1 Electronic structure

For a system where the d-electrons are well localized, and where the spin orbital interactions cannot be neglected, the GGA method is insufficient to describe such systems in particular the electronic properties. However, the GGA+U approach was initially suggested to describe correctly these later

systems. Then the Hubbard term (U) which describes the d–d or f–f interaction is added to the GGA energy. This method has proven its effectiveness for strongly correlated systems.

We notice that the band structures of spin-up states are similar to those for spin-down states. The electronic band structures of the monoclinic symmetry $KPdCu(Se_2)(Se_3)$ and $RbPdCu(Se_2)(Se_3)$ compounds are calculated. The calculated band structure profiles using GGA+U are shown in Fig. 2. We displayed the electronic band dispersion curves beside some high symmetry directions of the Brillouin zone (BZ) for $KPdCu(Se_2)(Se_3)$ and $RbPdCu(Se_2)(Se_3)$ compounds for the GGA+U approximation. We will consider only the EV-GGA consequences due to its improved band gap. The valence band maximum (VBM) and the conduction band minimum (CBM) are positioned at Y point of BZ, resulting in a direct energy band gap of about 1.258/1.275 $KPdCu(Se_2)(Se_3)$/$RbPdCu(Se_2)(Se_3)$. The calculated electronic structure of $KPdCu(Se_2)(Se_3)$ and $RbPdCu(Se_2)(Se_3)$ verifies that the investigated compounds are narrow-gap semiconductors. In order to illuminate the nature of the electronic band structures, we have calculated the total and partial density of states (TDOS and PDOS) for both compounds. Study of DOS using GGA+U approximation in both spin up and down states shows that there is no remarkable difference between the two states. These are presented in Fig. 3. Following Fig. 3, we should stress that there are three distinct structures separated by gaps. The first structure encountered in the TDOS, if we start from lower energies, consist entirely of K–p, Se-s and Rb-d states. These peaks are centered on around -14.0 to -10.0 eV for both compounds. The next structure, laying between -5.0 and 0.0 eV for both compounds consist of Pd-s/p, Cd-p/d and Se-p states. The conduction bands are comprised of Pd-s, Cu-s, Se-d, K-s and Rb-d states. From the PDOS we also concluded that at energy -5.0 eV, the Pd-s state forms a strong hybridization with the Se-p state. Near the Fermi level, Se-p state hybridize with Cu-p state, at the low conduction band Pd-s state strongly hybridize with Cu-s state.

3.2. Electron charge density

In order to establish a quantitative estimation for the type of bonding present in a particular molecule it is necessary to have a measure of the extent of charge transfer present in the molecule relative to the charge distributions of the separated atoms. To compute the phenomena of the bonding in the both investigated compound, we evaluated the atomic charge distribution along the investigated compound with the FPLAPW method based on the DFT. The electron density contours afford further approach

into the bonding interactions in the solid materials and to the bonding changes which consequence the changes in the DOS.

Now to understand the distribution of the total electronic charge density maps of $KPdCu(Se_2)(Se_3)$ and $KPdCu(Se_2)(Se_3)$ compounds, the valence electronic charge density (ECD) spectra have been depicted in Fig. 4 along (1 1 0) crystallographic plane. The crystallographic planes show there exists ionic and partial covalent bonding between K, Rb, Pd, Cu and Se atoms depending on Pauling electro-negativity difference i.e. higher the associated electro-negativity number, the more an element or compound attracts electrons towards it. The electro-negativity of K atom is (0.82), for Rb (0.79), for Pd (2.20), for Cu (1.90) and for Se (2.55) atoms. The atoms Pd-Se and Cu-Se form a weak covalent bonding and strong iconicity while K/Pd atoms exhibit pure ionic bonding. From these contour plots one can see that the majority of Pd and Cu electronic charge is transferred to Se atom. This can be seen easily by the color charge density scale where blue color (+1.0000) corresponds to the maximum charge accumulating site. The charge density along Pd and Se is pronounced. It is clear that when we replace K by Rb the charge density decreases. As it is clear from Fig. 4a, that the charge density around the Rb and Se is greater in $KPdCu(Se_2)(Se_3)$ compound than $RbPdCu(Se_2)(Se_3)$ compound.

3.3. Effective mass

We have calculated the effective mass of electrons (m_e^*) from the electronic band structure, since we are interested in the energy bands around the Fermi level (E_F) , therefore we have enlarged the band structure near E_F in order to show the bands which govern the energy band gap i.e. CBM and VBM. The effective mass of electrons (m_e^*) values were anticipated from the curvature of the conduction band minimum the band no.125 for $KPdCu(Se_2)(Se_3)$ compound and band no. 135 for $RbPdCu(Se_2)(Se_3)$, these bands are highlighted in different colors as shown in Fig. 2(e and f). The diagonal elements of the effective mass tensor, m_e, for the electrons in the conduction band are calculated in Γ→ Γ direction in k space using the following well-known relation:

$$\frac{1}{m_e^*} = \frac{1\partial^2 E(k)}{\hbar^2 \partial k^2} \quad \text{..... (5)}$$

The effective mass of electron is determined by fitting the electronic band structure to a parabolic function Eq. (5) in the first Brillouin zone using GGA+U approach. The effective mass of electron for the (symmetry) is obtained from the curvature of the conduction band at Γ- Γ point. The calculated

electron effective mass ratio (m_e^*/m_e) for $KPdCu(Se_2)(Se_3)$ and $RbPdCu(Se_2)(Se_3)$ in $\Gamma \rightarrow \Gamma$ direction is 0.0332 and 0.0225. It is obvious that the calculated value of $KPdCu(Se_2)(Se_3)$ is larger than $RbPdCu(Se_2)(Se_3)$ value. That is attributed to the fact that the parabolic curvature of $RbPdCu(Se_2)(Se_3)$ is greater than $KPdCu(Se_2)(Se_3)$, following the fact that the effective mass is inversely proportional to the curvature. We also have calculated the effective mass of the heavy holes i.e. the maximum valence band and light holes i.e. the second maximum valence band for $KPdCu(Se_2)(Se_3)$ and $RbPdCu(Se_2)(Se_3)$ compounds from the band number 134 and 133 (124 and 123) respectively. The calculated values of heavy holes and light holes for $KPdCu(Se_2)(Se_3)$ ($RbPdCu(Se_2)(Se_3)$) compounds are 0.1350 and 0.1858 (0.0202 and 0.0198).

3.4. Optical properties

The optical response functions of solids are frequently described by the complex dielectric function $\varepsilon(\omega) = \varepsilon_1(\omega) + i\varepsilon_2(\omega)$ or by the complex refractive index: $N(\omega) = n(\omega) + ik(\omega)$.

$$\varepsilon_1(\omega) = n^2 - k^2 \text{ ..... (6)}$$

$$\varepsilon_2(\omega) = 2nk \text{ ..... (7)}$$

In arguing the interaction between light and solid, one generally uses adiabatic approximation and single-electron approximation. Since the transition frequencies both in-band and between bands are much larger than the phonon frequency in the calculation of electronic structure and the method used is single-electron approximation, the phonon participation in the indirect transition process can be ignored, with only the electronic excitation considered. According to the definitions of direct transition probabilities and Kramers–Kronig dispersion relations, one can deduce the imaginary and the real parts of the dielectric function, absorption coefficient, reflectivity and complex optical conductivity [33–35] using:

$$\varepsilon_2(\omega) - = \frac{\pi e^2}{\varepsilon_0 m^2 \omega^2} \sum_{V,C} \{ \int_{BZ} \frac{2dk}{(2\pi)^2} \left| a \times M_{V,C} \right|^2 \delta[E_C(k) - E_V(k) - \hbar\omega] \} \text{ ..... (8)}$$

$$\varepsilon_1(\omega) = 1 + \frac{2e}{\varepsilon_0 m^2} \times \varepsilon_{V,C} \int_{BZ} \frac{2dk}{(2\pi)^2} \frac{\left| a \times M_{V,C}(k) \right|^2}{E_C(k) - E_V(k)/\hbar} \times \frac{1}{\left[E_C(k) - E_V(k) \right]^2 / \hbar^2 - \omega^2} \text{ ... (9)}$$

$$\alpha(\omega) = \frac{2k\omega}{c} = \frac{2\pi k}{\lambda_0} \text{ ..... (10)}$$

$$R(\omega)=\frac{(n-1)^2+k^2}{(n+1)^2+k^2} \ldots\ldots (11)$$

where 'n' is the refractive index, 'k' is the extinction coefficient, ε_0 is the vacuum dielectric constant, λ_0 is the wavelength of light in vacuum, C and V are the conduction band and valence band respectively, BZ is the first Brillouin zone, K is the electron wave vector, '**a**' is the unit direction vector of the vector potential A, M_{VC} is the transition matrix element, ω is the angular frequency, and $E_C(\omega)$ and $E_V(\omega)$ are the intrinsic energy level of the conduction band and valence band respectively.

Understanding of electronic structures can be reach by investigating the optical spectra which not only give reports about the occupied and unoccupied states, but also about the feature of the bands. Thus we intended to investigate the optical properties of $KPdCu(Se_2)(Se_3)$ and $RbPdCu(Se_2)(Se_3)$ compounds. Dielectric function as a connection connecting the microscopic physical transitions between bands to the electronic structures of a solid reflects the band structure of the solid and data about its spectrum. $KPdCu(Se_2)(Se_3)$ and $RbPdCu(Se_2)(Se_3)$ as a semiconductor materials, its spectrum generated by electronic transitions between the energy levels and all dielectric peaks can be explained using the calculated energy band structure and DOS. Fig. 5a and b, shows the spectrum of the real and imaginary parts of the complex dielectric function versus the photon energy. As it is clear from the above mentioned calculation that there is no remarkable difference in the electronic structure of spin-up states and spin-down states. So here we will discuss the optical properties only using the spin up states. Our analysis of $\varepsilon_2(\omega)$ spectrum (Fig. 5a) shows that the first critical point of the dielectric function occurs at 0.30 eV. This point is $Y_v \rightarrow Y_c$, which gives the threshold for the optical transitions between the VBM and the CBM. This is known as the fundamental absorption edge. Beyond this threshold energy (first critical point), the curve increases rapidly. This is due to the fact that the number of points contributing towards $\varepsilon_2(\omega)$ is increased abruptly. Since the investigated compounds have monoclinic symmetry, thus only three tensor components are exists to describe all the optical properties. These are $\varepsilon_2^{xx}(\omega)$, $\varepsilon_2^{yy}(\omega)$ and $\varepsilon_2^{zz}(\omega)$. The main peak of $\varepsilon_2^{xx}(\omega), \varepsilon_2^{yy}(\omega)$ and $\varepsilon_2^{zz}(\omega)$ spectrum is situated at about 2.0 eV. The observed structure at Fig. 5a, show there exists a second pronounced peak and three humps as shown in Fig.5 a and b.

The real part of $\varepsilon_1(\omega)$, can be obtained by using the Kramers Kronig transformation. The results for the dispersive part of the dielectric function, $\varepsilon_1(\omega)$ for the compounds under investigation are

illustrated in Fig. 5 c and d. The main features in this spectrum is the peak at around 1.8 eV, the rather steep decrease below 9.0 eV, after which $\varepsilon_1(\omega)$ becomes negative, and the minimum followed by a slow increase toward zero at high energies. In the energy range where $\varepsilon_1(\omega)$ is negative, the electromagnetic wave will not be propagated. For the real dielectric function, the most important quantity is the zero frequency limits $\varepsilon_1(0)$, since it gives the static dielectric constant in the zero frequency limits, which has the value 6.168 (5.908), 6.240 (5.994) and 6.149 (5.718) of $\varepsilon_1^{xx}(0)$, $\varepsilon_1^{yy}(0)$ and $\varepsilon_1^{zz}(0)$ for KPdCu(Se_2)(Se_3) (RbPdCu(Se_2)(Se_3)).

Fig. 6(a–h) shows the energy loss function $L(\omega)$, reflectivity $R(\omega)$, refractivity $n(\omega)$ and the absorption coefficient $I(\omega)$. The complex refractive index ($\tilde{n}(\omega) = n(\omega) + ik(\omega)$) portray the refraction and also the absorption of the compounds. It contains two parts; the real part, $n(\omega)$, is the refractive index second-order tensor whereas the other part, $k(\omega)$, is the extinction tensor which illustrates the loss of photon energy throughout propagation during the optical medium. The premeditated refractive index for KPdCu(Se_2)(Se_3) and RbPdCu(Se_2)(Se_3), are illustrated in Figs. 6(a and b). The calculated non zero tensor components of static refractive index $n^{xx}(0)$, $n^{yy}(0)$ and $n^{zz}(0)$ are 2.483, 2.498 and 2.479 for KPdCu(Se_2)(Se_3) and 2.430, 2.448 and 2.391 for KPdCu(Se_2)(Se_3). According to Penn's model [36] that $\varepsilon_1(0)$ relates to band gap of the material and $\varepsilon_1(0)$ is directly related to the n (0) by the relation $n(\omega) = \sqrt{\varepsilon_1(0)}$. They are improved beyond the zero frequency limits accomplishing their maximum values. Further than the maximum value start to decrease and with few oscillations go beyond unity. In this region (n<1) the phase velocity of the photons enhances approaching to universal constant (C). On the other hand the group velocity always remnants less than the C, as a significance the relativity relations are not affected [37]. The spectrum is moved towards inferior energy by altering the cations from K to Rb. The distinction is in agreement to the lessening in the band gap. The absorption spectra of KPdCu(Se_2)(Se_3) and RbPdCu(Se_2)(Se_3) (Figs. 6 c and d) demonstrate that these materials initiate absorbing the radiation at the 2.0 eV for both compounds. The absorption spectra show the uppermost value at 13.6 eV analogous to the minimum value of $\varepsilon_1(\omega)$ and $\varepsilon_2(\omega)$ shown in Fig.5a-d.

The frequency dependent reflectivity $R^{xx}(\omega)$, $R^{yy}(\omega)$ and $R^{zz}(\omega)$ are calculated and depicted in Figs. 6 (e and f). The reflectivity spectra of the compounds originates from the zero energy which

characterizes the static part of the reflectivity components $R^{zz}(0)$, $R^{yy}(0)$ and $R^{xx}(0)$. These values are equal to 0.173, 0.176 and 0.168 for KPdCu(Se_2)(Se_3) compound and 0.181, 0.183 and 0.180 for RbPdCu(Se_2)(Se_3) compound. The energy loss function $L^{xx}(\omega)$, $L^{yy}(\omega)$ and $L^{zz}(\omega)$, as illustrated in Fig. 6 g and h, is a key component for the evaluation of the use fullness of very quick going electron's energy of the material. The sharp spectral peaks produced in $L^{xx}(\omega)$, $L^{yy}(\omega)$ and $L^{zz}(\omega)$ around 11.8 eV for KPdCu(Se_2)(Se_3) and at 12.0 eV for RbPdCu(Se_2)(Se_3) are due to the occurrence of plasmon excitations [38]. It is observed that the relative maximum in the energy loss function occurs with good approximation at energies where the dielectric function $\varepsilon_1(\omega)$ has the root.

3.5. Thermal properties

The main intend of this manuscript is to work out the thermoelectric properties of APdCu(Se_2)(Se_3) (A= K and Rb) and its distinction varying with temperature. It is essential to guesstimate the effective masses of the carriers in different electron and hole pockets to attain this task. We have computed the effective mass (electron, heavy hole and light hole) ratio of the carriers at the conduction and valence band edges by fitting the energy of the respective bands to a quadratic polynomial in the reciprocal lattice vector $\tilde{k}$ as discussed in the above section 3.3. It is pretty apparent that the bands are less dispersive in the KPdCu(Se_2)(Se_3) structure approximately in all the high symmetry directions. That's why we entailed large effective mass and hence entailing to get a high thermo-power. Though, existence of carriers with huge mobility is essential for attaining a higher electrical conductivity. Thus there is an opportunity of gaining large figure of merit (ZT) factor in these compounds having multiple pockets of carriers with considerable and minute effective masses with the former one leading to large Seebeck coefficient (S), and the latter one improving $\sigma(\tau)$ [39,40]. It is motivating to memo that the electronic structure of the investigated compounds exposes existence of multiple carrier pockets with significantly dissimilar effective masses thereby signifying that they may be having good thermoelectric properties.

For the conductivity coefficient calculation, the relaxation time term τ should be treated as a constant parameter. Fig. 7(a and b) presents the calculated temperature dependent electrical conductivities for new quaternary copper palladium polyselenides with monoclinic symmetry as a function of relaxation time $\sigma(\tau)$ within the temperature interval from 300K to 800 K, which is denoted as σ^{xx}, σ^{yy} and σ^{zz} components. It is found that the conductivity as a function of relaxation time is anisotropic.

Assuming that the relaxation time τ is direction independent, the value of σ^{xx} and σ^{zz} components at 800K are two times smaller than value of σ^{yy} component.

The σ^{xx}, σ^{yy} and σ^{zz} values increase rapidly along with increasing temperature, confirming the semiconductor like transportation and temperature sensitive conduction, this is in good agreement with calculated electronic band structure. The anisotropic nature should be enhanced at higher temperature, as is shown with in Fig. 7(a and b). Though there is anisotropy in the σ^{xx}, σ^{yy} and σ^{zz} at 300 K but this anisotropy is much greater at high temperature. The maximum conductivity values as a function of relaxation time reach to $6\times10^{18}\Omega^{-1}m^{-1}s^{-1}$, $1.72\times10^{18}\Omega^{-1}m^{-1}s^{-1}$ and $4.8\times10^{18}\Omega^{-1}m^{-1}s^{-1}$ within σ^{xx}, σ^{yy} and σ^{zz} components, respectively for $KPdCu(Se_2)(Se_3)$. In the $KPdCu(Se_2)(Se_3)$ compound the σ^{xx} and σ^{zz} components shows weak anisotropy with increasing temperature up to 550K, then the anisotropy increases with increasing the temperature. The anisotropy between σ^{xx} and σ^{zz} components is comparatively very smaller than that of σ^{xx} and σ^{zz} with the σ^{yy} component. As we replace K by Rb, in both compounds the conductivity increases with the increasing the temperature. In $RbPdCu(Se_2)(Se_3)$ there exists isotropy between σ^{xx} and σ^{zz} components within the whole range of temperature. While σ^{xx} and σ^{zz} components shows considerable anisotropy with the σ^{yy} component. The maximum conductivity values for $RbPdCu(Se_2)(Se_3)$ as a function of relaxation time reach to $0.5\times10^{18}\Omega^{-1}m^{-1}s^{-1}$ for σ^{xx} and σ^{zz} components, and about $6.85\times10^{18}\Omega^{-1}m^{-1}s^{-1}$ for σ^{yy} component. From the conductivity spectra of both compounds we concluded that the $KPdCu(Se_2)(Se_3)$ compound shows greater increase in conductivity than $KPdCu(Se_2)(Se_3)$ compound.

Fig. 7 (c and d) presents the calculated temperature dependent Seebeck coefficients (S) for $APdCu(Se_2)(Se_3)$ (A =K and Rb) compounds within the temperature interval from 300K to 800 K, which is denoted as S^{xx}, S^{yy} and S^{zz} components. It is found that the Seebeck coefficient as a function of temperature is also anisotropic, the Seebeck coefficient within S^{xx}, S^{yy} and S^{zz} components show reverse behaviors as a function of temperature comparing with that of the conductivity.

For example, the S value within 'S^{yy}' component is larger than that within the S^{xx} and S^{zz} components and the anisotropic nature remains the same in the higher temperature region. The values of S^{xx}, S^{yy} and S^{zz} components show positive temperature dependence, and it could also be observed that the values of S^{xx}, S^{yy} and S^{zz} tends to be completely soaked at high temperature region, reaching to 1.83 (2.16)$\times10^{-4}$, 1.57 (1.97) $\times10^{-4}$ and 1.55 (1.59) $\times10^{-4}$ for S^{xx}, S^{yy} and S^{zz} components,

respectively, for $KPdCu(Se_2)(Se_3)$ ($RbPdCu(Se_2)(Se_3)$) compounds at 800K temperature. Furthermore, in consideration of the conductivity dependence as a function of temperature, the electrical performance should be enhanced with elevating the temperature.

As we replace K by Rb the decrease in the Seebeck coefficient for both the compounds is the same with increasing the temperature. The three components show considerable anisotropy with increasing temperature in both compounds. If we gaze to the spectra with increasing temperature the S^{xx}, S^{yy} and S^{zz} components decrease, but the S^{xx} component shows different behavior than the S^{yy} and S^{zz} components. The decrease in S^{xx} component is till 600K and shows equilibrium at 650 K and then start to increase with increasing temperature. At low temperature $RbPdCu(Se_2)(Se_3)$ compound shows greater value of Seebeck coefficient than the that of $KPdCu(Se_2)(Se_3)$ compound.

Fig. 7 (e and f) presents the calculated temperature dependent power-factor (PF) as a function of relaxation time with in the temperature interval from 300K to 800K, which is denoted as P^{xx}, P^{yy} and P^{zz}. The PF value within P^{xx}, and P^{zz} components at 800K are almost two times smaller than that value of P^{yy} component assuming that the relaxation time τ is direction independent. The PF values increase rapidly along with increasing temperature, confirming the electrical performance is sensitive to temperature. The anisotropic nature is enhanced at higher temperature, as shown in Fig. 7 (e and f). In $KPdCu(Se_2)(Se_3)$ compound the P^{xx}, and P^{zz} components exhibit weak anisotropy in low temperature but the anisotropy increases with increasing the temperature, the anisotropy between these two components is comparatively very smaller than that along the P^{yy} component. Whereas in the $RbPdCu(Se_2)(Se_3)$ compound the P^{xx}, and P^{zz} components shows isotropy up to 550 K which increases with the increasing temperature then both of P^{xx}, and P^{zz} components shows considerable anisotropy with the P^{yy} component. We should emphasize that the $KPdCu(Se_2)(Se_3)$ compound shows greater power-factor value than that obtained from $KPdCu(Se_2)(Se_3)$ compound. The maximum power-factor values as a function of relaxation time are reaches to 4.3 (3.5)$\times 10^{11}$, 2.0 (1.57) $\times 10^{11}$ and 1.2 (1.5) $\times 10^{11}$ W/mK^{-2}s for P^{xx}, P^{yy} and P^{zz} components, respectively for $KPdCu(Se_2)(Se_3)$ ($RbPdCu(Se_2)(Se_3)$) compounds. From the analysis of both compounds, we concluded that both compounds possess good thermoelectric properties at high temperature, but $KPdCu(Se_2)(Se_3)$ shows much better thermoelectric behavior than $RbPdCu(Se_2)(Se_3)$, that is attributed to the fact that at higher temperature $KPdCu(Se_2)(Se_3)$ compound shows good PF value than $RbPdCu(Se_2)(Se_3)$ compound.

4. Conclusions

In summary, the electronic band structure, optical properties and electrical transport coefficients of $APdCu(Se_2)(Se_3)$ (A= K and Rb) a new quaternary copper palladium polyselenides have been studied. From the study of electronic band structure we concluded that the valence band maximum (VBM) and the conduction band minimum (CBM) are positioned at Y point, resulting in a direct energy band gap of about 1.258/1.275 eV. From the PDOS we also concluded that at energy -5.0 eV, the state Pd-s strongly hybridize with the Se-p state. Near the Fermi level, Se-p state hybridize with Cu-p state, and at the low conduction band Pd-s forms a strong hybridization with Cu-s. We also have calculated the electronic charge density in the (010) plane, one can see that the Pd-Se and Cu-Se atoms forms weak covalent bonding and strong iconicity, while K/Pd atoms exhibit pure ionic bonding. We also have calculated the effective mass ratio of the electron, heavy holes and light holes. The calculated effective mass ratio for electron, heavy holes and light holes for $KPdCu(Se_2)(Se_3)$/($RbPdCu(Se_2)(Se_3)$) are 0.0332/(0.0225), 0.1350/(0.0202) and 0.1858/(0.0198) respectively. The real and imaginary parts of dielectric function and hence the optical constants such as refractive index and extinction coefficient are calculated and discussed in details. From the absorption spectrum we concluded that both of KPdCu(Se2)(Se3) and RbPdCu(Se2)(Se3) compounds demonstrate that these materials initiate absorbing the radiation at around 1.8 - 2.0 eV. The absorption spectra show the uppermost value at 13.6 eV analogous to the minimum value of $\varepsilon_1(\omega)$ and $\varepsilon_2(\omega)$. The Seebeck coefficient together with the conductivity and the power-factor as a function of relaxation time are calculated systematically. The calculated conductivity and Seebeck coefficient confirm its anisotropic nature and the semiconductor transport behavior. The calculated power-factor as a function of relaxation time increases rapidly with increasing temperature. The maximum power-factor values as a function of relaxation time reach to 4.3 (3.5)$\times 10^{11}$, 2.0 (1.57) $\times 10^{11}$and 1.2 (1.5) $\times 10^{11}$W/mK^{-2}s for P^{xx}, P^{yy} and P^{zz} components, respectively for $KPdCu(Se_2)(Se_3)$ ($RbPdCu(Se_2)(Se_3)$) at 800K. The present calculation of TE behaviors of $APdCu(Se_2)(Se_3)$ (A= K and Rb) for the power-factor signifies that both compounds show good thermoelectric properties at high temperature.

AKNOWLEDEGMENT

The result was developed within the CENTEM project, reg. no. CZ.1.05/2.1.00/03.0088, co-funded by the ERDF as part of the Ministry of Education, Youth and Sports OP RDI programme. School of Material Engineering, Malaysia University of Perlis, Malaysia

References

[1] (a) H. Eckert, and Angew Chem. Int. Ed. Engl. 28, 1723 (1989) (b) Y. Wang, N. Herron, W. Mahler, and A. Suna, J. Opt. Soc. Am. 6B, 808 (1989) (c) R. Chung, T. Hogan, P. Brazis, M. Rocci-Lane, C. Kannewurf, M. Bastea, C. Uher, and M. G. Kanatzidis, Science 287, 1024 (2000)

[2] W. S. Sheldrick, and M. Wachhold, Coord. Chem. ReV. 176, 211 (1998)

[3] M. G. Kanatzidis, and A. C. Sutorik, Prog. Inorg. Chem. 43, 151 (1995)

[4] M. G. Kanatzidis, Curr. Opin. Solid State Mater. Sci. 2, 139 (1997)

[5] M. G. Kanatzidis, and B. K. Das, Comments Inorg. Chem. 21, 29 (1999)

[6] W. S. Sheldrick, and M. Wachhold, Angew. Chem., Int. Ed. Engl. 36, 206 (1997)

[7] G. Kra¨uter, and K. Dehnicke, Chem.-Ztg. 114, 7-9 (1990)

[8] K.-W. Kim, and M. G. Kanatzidis, J. Am. Chem. Soc. 120, 8124-8135 (1998).

[9] M. Wachhold, and M. G. Kanatzidis, J. Am. Chem. Soc. 121, 4189-4195 (1999)

[10] K.-W. Kim, and M. G. Kanatzidis, J. Am. Chem. Soc. 114, 4878 (1992)

[11] J. Li, Z. Chen, R.-J. Wang, and J. Y. J. Lu, Solid State Chem. 140, 149 (1998)

[12] J. Llanos, C. Contreras-Ortega, C. Mujica, H. G. von Schnering, and K. Peters, Mater. Res. Bull. 28, 39-44 (1993)

[13] C. Mujica, J. Paez, and Llanos, J. Mater. Res. Bull. 29, 263-268 (1994)

[14] J. Li, H.-Y. Guo, R. A. Yglesias, and T. Emge, J. Chem. Mater. 7, 599-601 (1995)

[15] J. Llanos, C. Contreras-Ortega, J. Paez, M. Guzman, and C. Mujica, J. Alloys Compd. 201, 103-104 (1993)

[16] J. Llanos, P. Valenzuela, C. Mujica, A. Buljan, and R. Ramirez, J. Solid State Chem. 122, 31-35 (1996)

[17] Xuean Chen, Kieran J. Dilks, Xiaoying Huang, and Jing Li. Inorganic Chemistry, 42, 3723-3727 (2003)

[18] P. Guss, Michael E. Foster, Bryan M. Wong, F. Patrick Doty, Kanai Shah, Michael R. Squillante, Urmila Shirwadkar, Rastgo Hawrami, Joshua Tower, Ding Yuan, J. Appl. Phys., 115, 034908 (2014).

[19] V. I. Anisimov F. Aryasetiawan, A. I. Lichtensteinet, J. Phys.: Condens. Matter 9, 767 (1997)

[20] John P. Perdew, B. Kieron, E. Matthias, Phys. Rev. Lett. 77 (October) (1996)

[21] P. Hohenberg, and W. Kohn. Phys. Rev. 136, B864 (1996)

[22] W. Kohn, and L. J. Shom. Phys. Rev. 140, A1133 (1965)

[23] P.Blaha, K. Schwarz, and J. Luitz WIEN97, A full potential linearized augmented plane wave package for calculating crystal properties, Karlheinz Schwarz. Techn. Universit at Wien, Austria, 1991. ISBN:3-9501031-0-4.

[24] C. Loschen, J. Carrasco, K.M. Neyman, F. Illas, Phys. Rev. B 75 (2007) (2007) 035115.].

[25] J.C. Li, C.L. Wang, M.X. Wang, H. Peng, R.Z. Zhang, M.L. Zhao, J. Liu, J.L. Zhang, and L.M. Mei, J. Appl. Phys. 105, 043503 (2009)

[26] A. Popescu, L.M. Woods, J. Martin, and G.S. Nolas, Phys. Rev. B 79, 205302 (2009)

[27] M. Zebarjadi, K. Esfarjani, M. S. Dresselhaus, Z. F. Ren, and G. Chen, Energy Environ. Sci. 5, 5147 (2012).

[28] L. Bertini, and C. Gatti, J.Chem.Phys.121, 8983 (2004)

[29] Y. Wang, X. Chen, T. Cui, Y. Niu, Y. Wang, M. Wang, Y. Ma, and G. Zou, Phys. Rev. B 76, 155127 (2007)

[30] L. Lykke, B. B. Iversen, and G. K. H. Madsen, Phys.Rev.B 73, 195121 (2007)

[31] A. Zunger, R. Hull, R. M. Osgood, and H. Sakaki, Springer-Verlag,Berlin, 68.

[32] G. K. H. Madsen, and D. J. Singh,Comput.Phys.Commun.175, 67 (2006)

[33] R. C. Fang, Spectroscopy of Solid, University of Science and Technology Press, Hefei, China, 71–75 (2001)

[34] X. J Sheng, Science Press, Beijing, 76–94 (2002)

[35] Q. Chen, Q. Xie, and W.J. Yan, Sci. China (Ser. G) 38 (7): 825–833 (2008)

[36] D.R. Penn, Phys. Rev. B.128, 2093-2097 (1962)

[37] M. Fox, Optical Properties of Solids, Oxford University Press, (2001)

[38] L. Marton, Rev. Mod. Phys. 28, 172-184 (1956)

[39] D. Parker, and D. J. Singh. *Phys. Rev. B.* 85, 125209-1-7 (2012)

[40] D. J. Singh, and I. I. Mazin, *Phys.Rev. B. 56*, R1650-R1653 (1997).

Tables Caption

Table 1: Bond lengths (Å)

Table 2: Bond angles (˚)

Figures Caption

Fig. 1: Unit cell structure

Fig. 2: Calculated band structure.

Fig. 3: Calculated total and partial densities of states (States/eV unit cell)

Fig. 4: Electronic charge density contour.

Fig. 5: Calculated imaginary $\varepsilon_2(\omega)$ and real part $\varepsilon_1(\omega)$ of dielectric tensor

Fig. 6: Calculated refractivity $n(\omega)$, absorption coefficient $I(\omega)$, reflectivity $R(\omega)$ and the energy-loss function spectrum $L(\omega)$.

Fig. 7: Calculated thermoelectric properties; Seebeck coefficients, electrical conductivity and power factor.

Table 1: Bond lengths

KPdCu(Se2)(Se3)	Opt.	Exp.	RbPdCu(Se2)(Se3)	Opt.	Exp.
Cu- Se4	2.3657	2.369(1)	Pd- Se4	2.4760	2.454(2)
Cu- Se1	2.4571	2.467(2)	Cu- Se4	2.3598	2.362(2)
Cu- Se3	2.3765	2.411(2)	Cu- Se3	2.3748	2.411(4)
K-Se3	3.4387	3.458(4)	Cu- Se1	2.4583	2.479(3)
Pd- Se1	2.4723	2.4515(9)	Se1- Se2	2.3794	2.337(4)
Pd- Se4	2.4758	2.458(1)	Se3- Se4	2.4441	2.383(2)
Se1- Se2	2.3851	2.338(2)	Rb- Se2	3.4140	3.407(3)
K- Se4	3.4121	3.423(3)	Rb- Se2	3.6681	3.420(3)
K- Se2	3.6625	3.6656(7)	Rb- Se2	3.6681	3.6702(7)
K- Se2	3.3297	3.349(4)	Rb- Se3	3.5010	3.524(4)
K- Se2	3.2941	3.299(3)	Pd- Se1	2.4746	2.455(2)
Se3- Se4	2.4484	2.390(1)	Rb- Se4	3.6209	3.525(3)
K- Se4	3.5072	3.541(3)	Rb- Se4	3.5089	3.656(3)

Table 2: Bond angles

KPdCu(Se2)(Se3)	Exp.	Opt.	RbPdCu(Se2)(Se3)	Exp.	Opt.
Se(1)-Pd-Se(4)	87.20(4)	87.22	Se(4)-Pd-Se(1)	87.55(7)	87.47
Se(1)-Pd-Se(4)	92.80(4)	92.78	Se(4)-Pd-Se(1)	92.45(7)	92.53
Se(1)-Pd-Se(1)	180	180	Se(1)-Pd-Se(1)	180	180
Se(4)-Pd-Se(4)	180	180	Se(4)-Pd-Se(4)	180	180
Se(3)-Cu-Se(1)	85.19(7)	85.48	Se(3)-Cu-Se(1)	84.6(1)	85.15
Se(4)-Cu-Se(4)	108.08(8)	106.77	Se(4)-Cu-Se(4)	107.8(1)	106.16
Se(4)-Cu-Se(1)	112.06(6)	111.11	Se(4)-Cu-Se(1)	114.2(1)	113.60
Se(4)-Cu-Se(3)	118.77(5)	120.15	Se(4)-Cu-Se(3)	117.4(1)	118.69
Se(4)-Se(3)-Se(4)	91.78(6)	90.26	Se(4)-Se(3)-Se(4)	92.8(1)	91.24
Se(3)-Se(4)-Pd	107.53(5)	106.20	Se(3)-Se(4)-Pd	107.74(9)	106.21
Se(2)-Se(1)-Pd	111.05(4)	109.65	Se(2)-Se(1)-Pd	110.73(8)	109.25
Pd-Se(1)-Pd	95.67(5)	94.60			

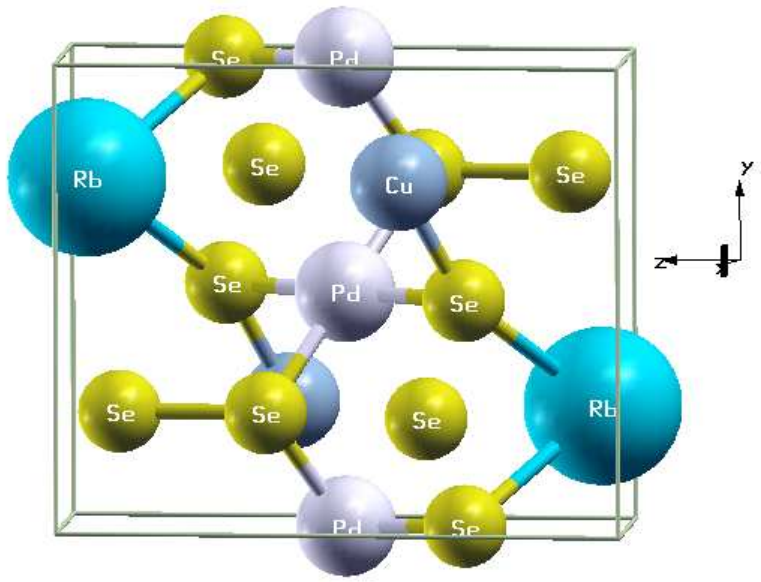

(a) RbPdCu(Se_2)(Se_3) unit cell structure

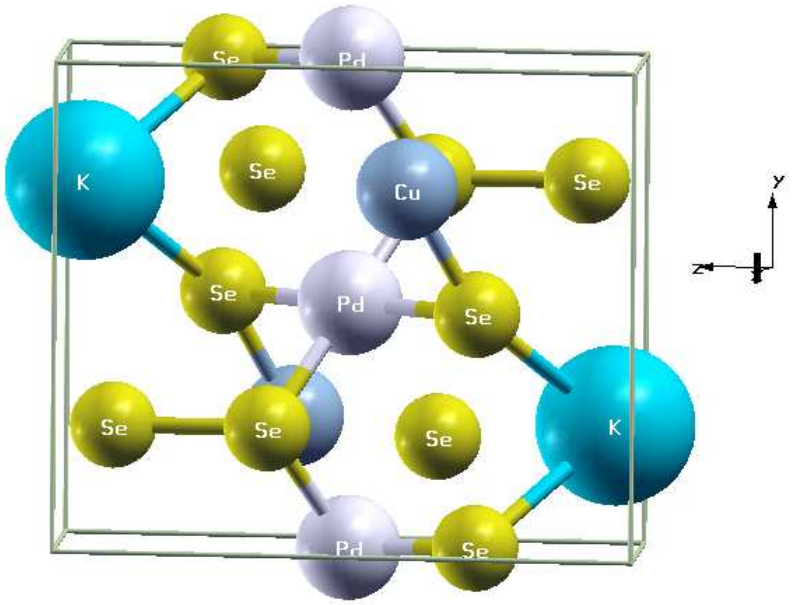

(b) $KPdCu(Se_2)(Se_3)$ unit cell structure

Fig. 1:

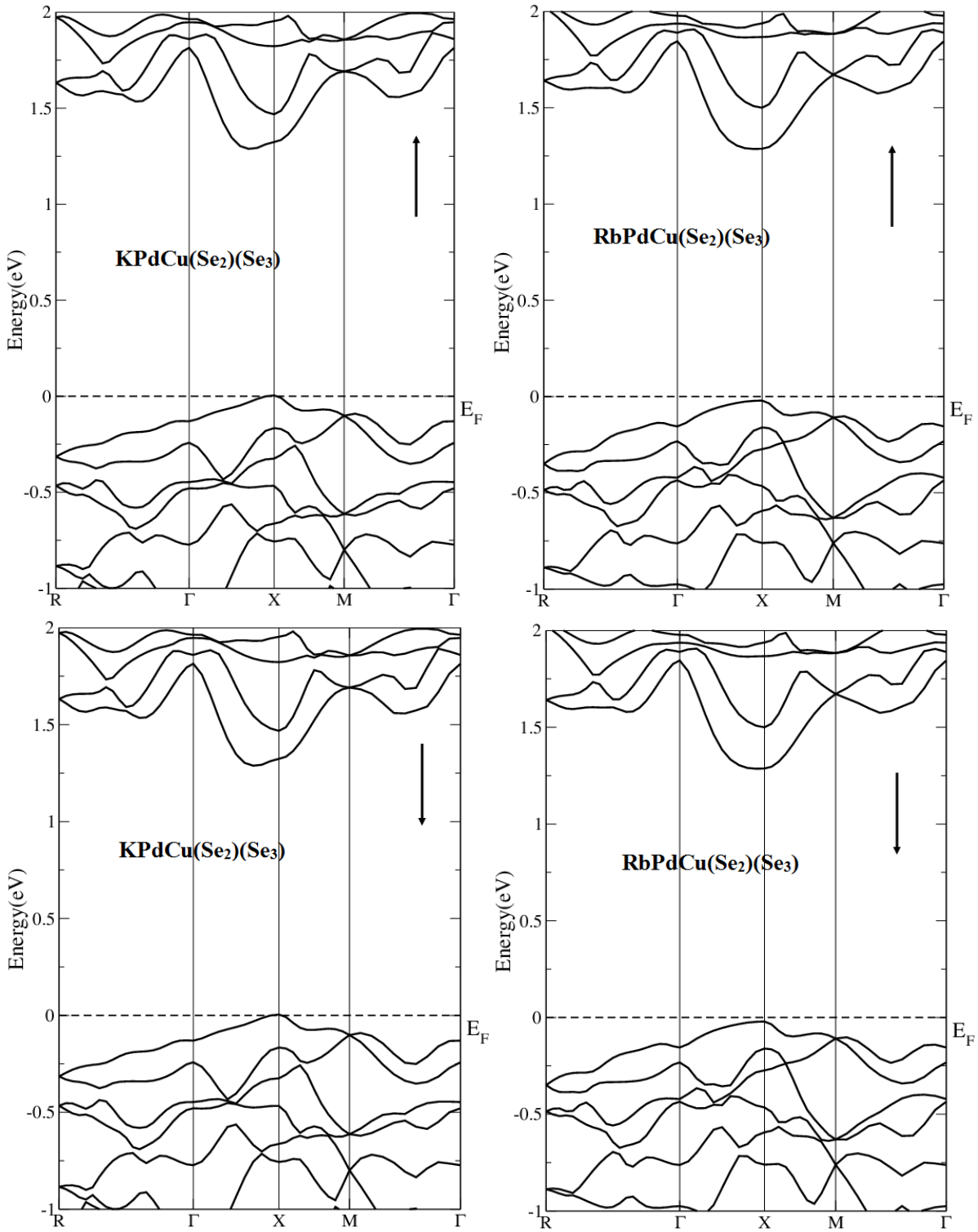
KPdCu(Se2)(Se3)
RbPdCu(Se2)(Se3)
KPdCu(Se2)(Se3)
RbPdCu(Se2)(Se3)
Energy(eV)
E_F
R
Γ
X
M
Γ

Fig. 2

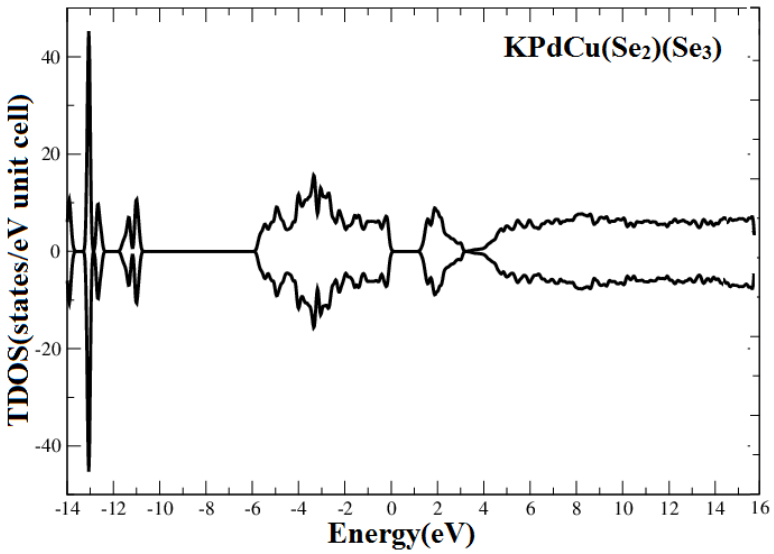
KPdCu(Se2)(Se3)
TDOS(states/eV unit cell)
Energy(eV)
40
20
0
-20
-40
-14
-12
-10
-8
-6
-4
-2
0
2
4
6
8
10
12
14
16

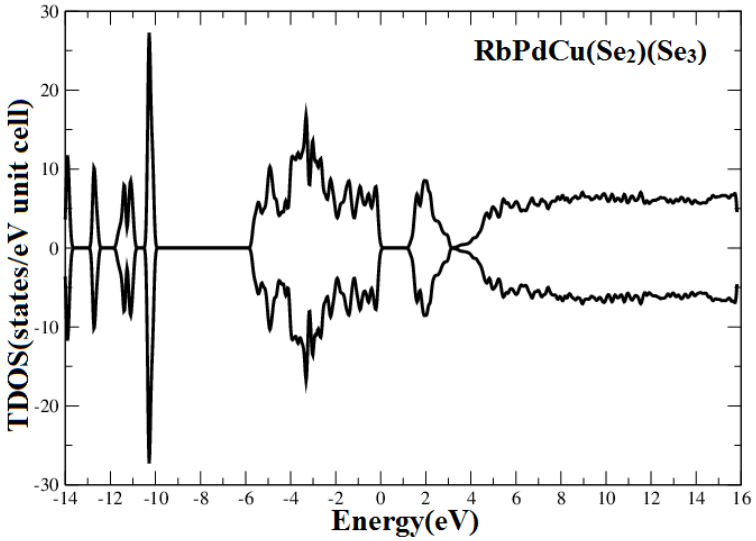
RbPdCu(Se2)(Se3)
TDOS(states/eV unit cell)
Energy(eV)
30
20
10
0
-10
-20
-30
-14
-12
-10
-8
-6
-4
-2
0
2
4
6
8
10
12
14
16

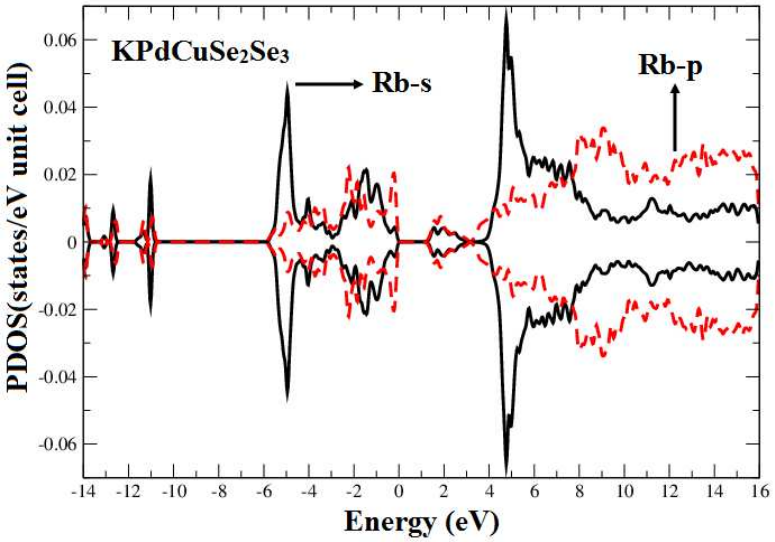
KPdCuSe2Se3
Rb-s
Rb-p
PDOS(states/eV unit cell)
Energy (eV)

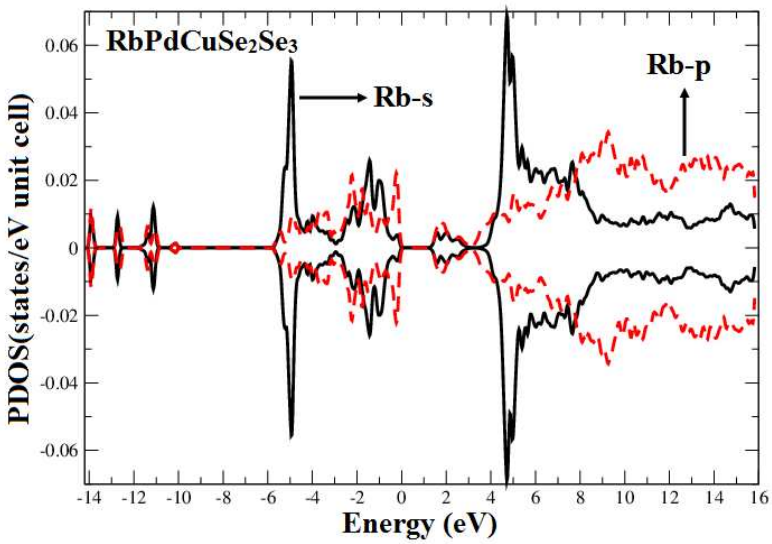
RbPdCuSe2Se3
Rb-s
Rb-p
PDOS(states/eV unit cell)
Energy (eV)

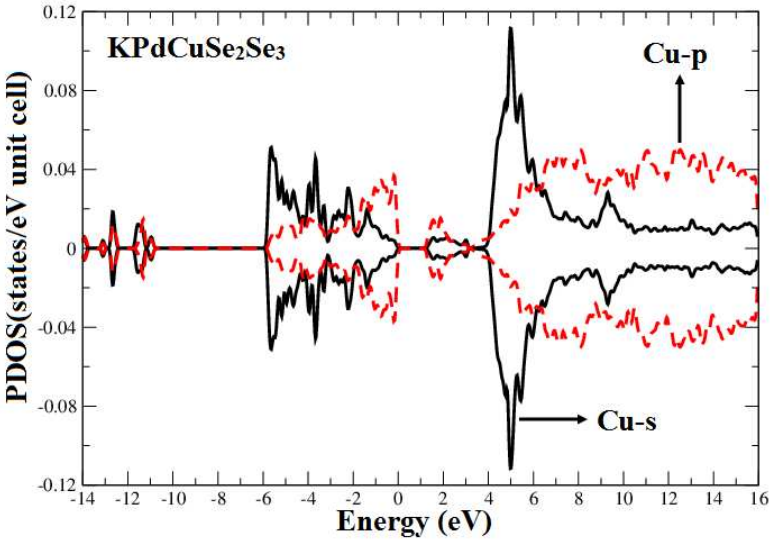
KPdCuSe2Se3
Cu-p
Cu-s
PDOS(states/eV unit cell)
Energy (eV)

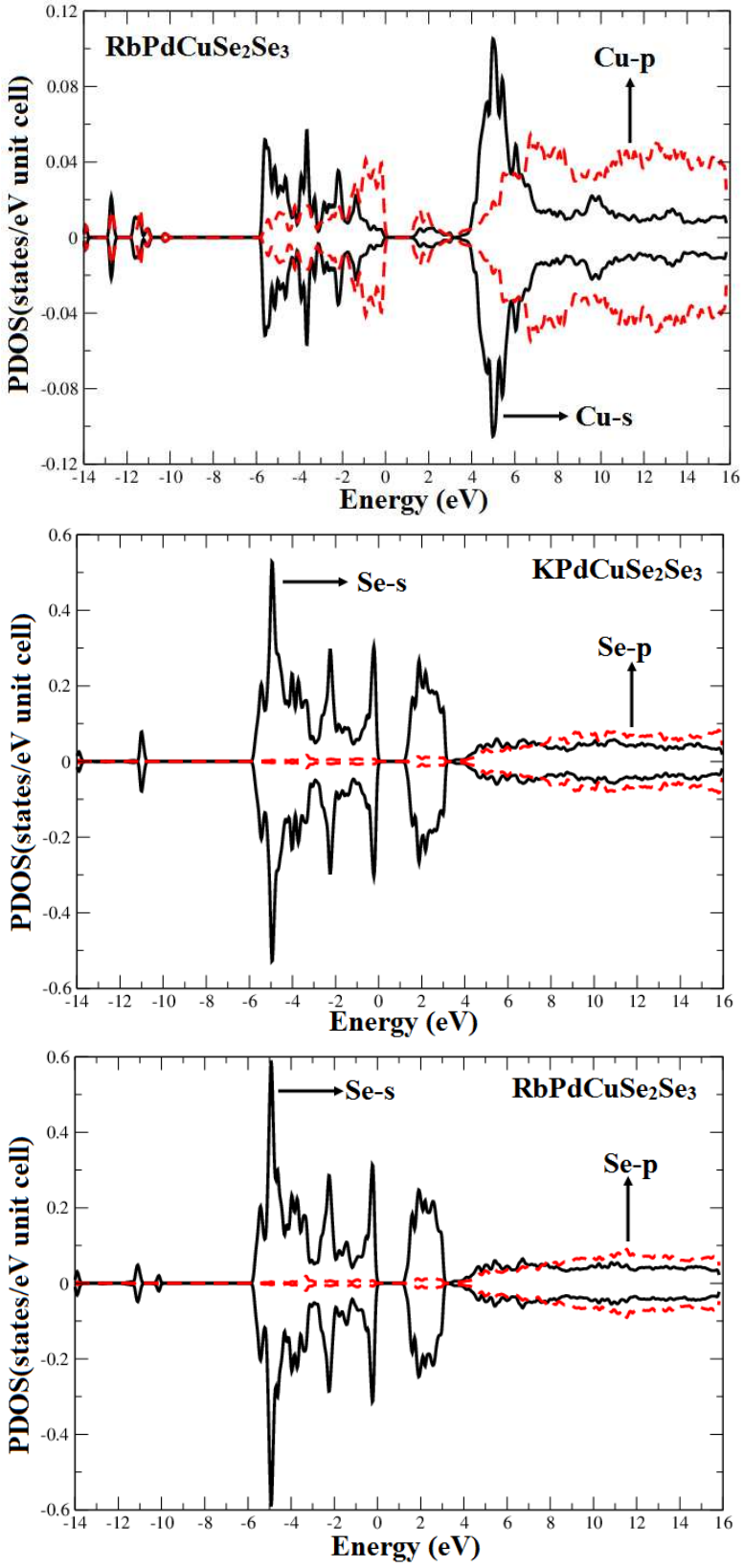
RbPdCuSe2Se3
Cu-p
Cu-s
PDOS(states/eV unit cell)
Energy (eV)
KPdCuSe2Se3
Se-s
Se-p
PDOS(states/eV unit cell)
Energy (eV)
RbPdCuSe2Se3
Se-s
Se-p
PDOS(states/eV unit cell)
Energy (eV)

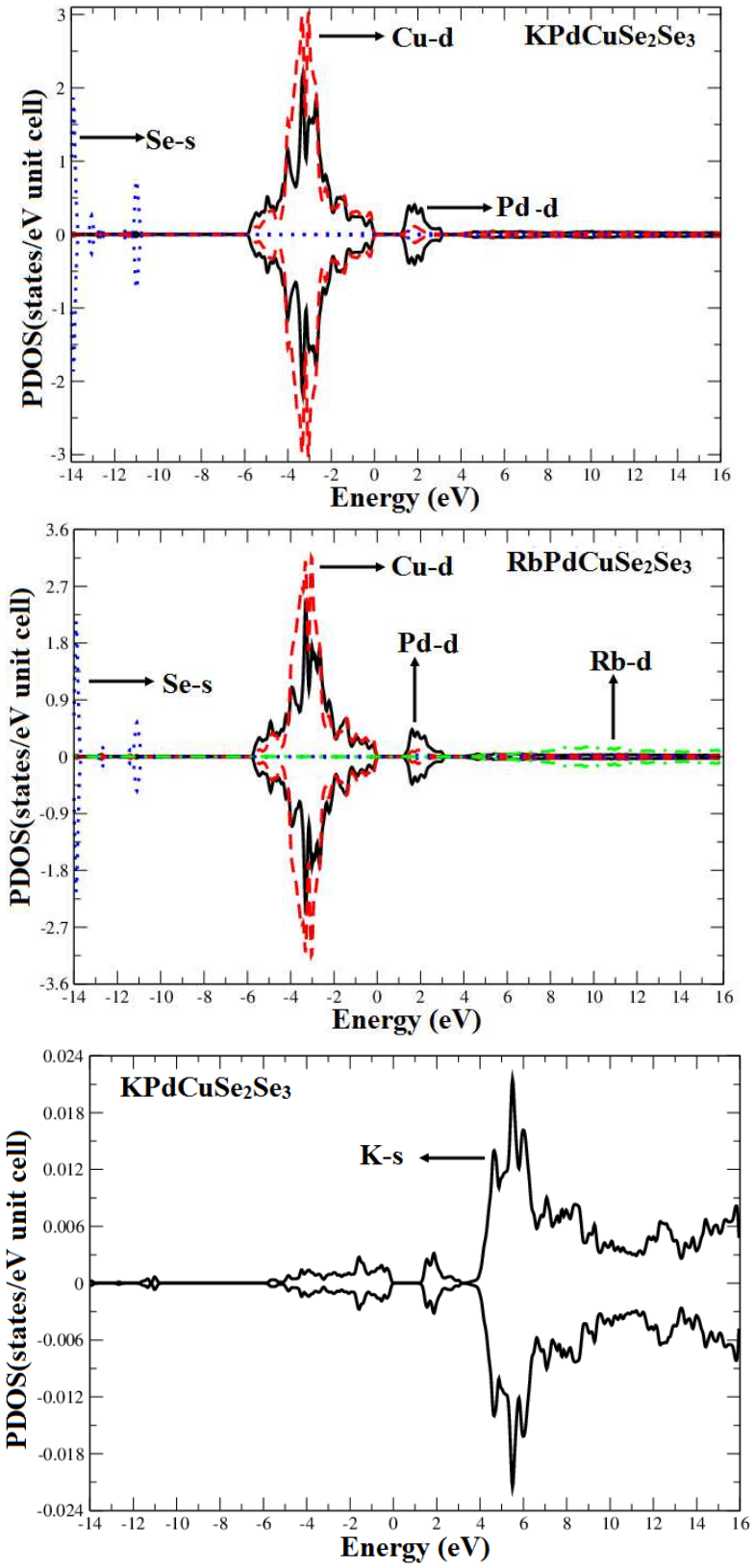
Cu-d
KPdCuSe2Se3
Se-s
Pd -d
PDOS(states/eV unit cell)
Energy (eV)
Cu-d
RbPdCuSe2Se3
Pd-d
Rb-d
Se-s
PDOS(states/eV unit cell)
Energy (eV)
KPdCuSe2Se3
K-s
PDOS(states/eV unit cell)
Energy (eV)

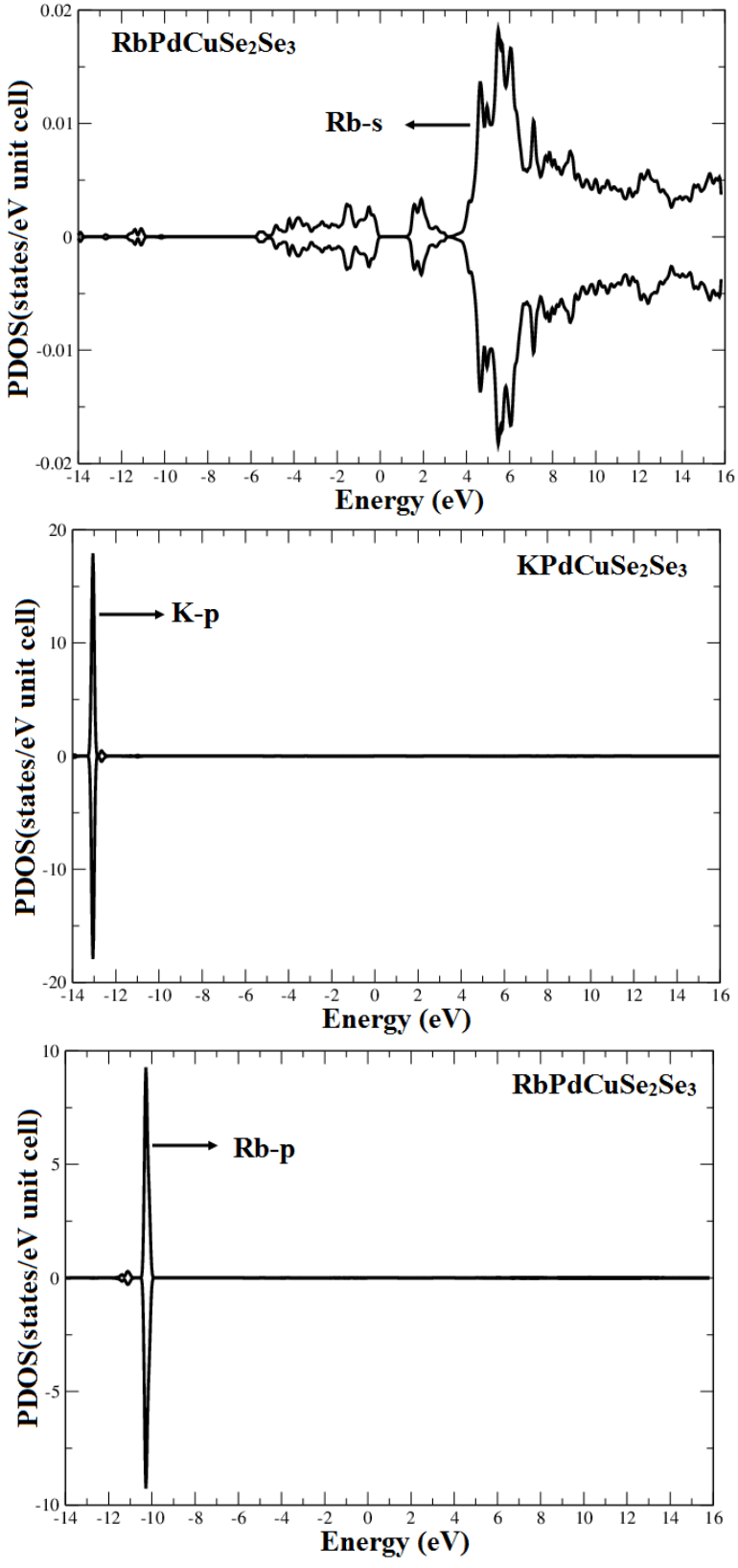
RbPdCuSe2Se3
Rb-s
PDOS(states/eV unit cell)
Energy (eV)
KPdCuSe2Se3
K-p
PDOS(states/eV unit cell)
Energy (eV)
RbPdCuSe2Se3
Rb-p
PDOS(states/eV unit cell)
Energy (eV)

Fig. 3:

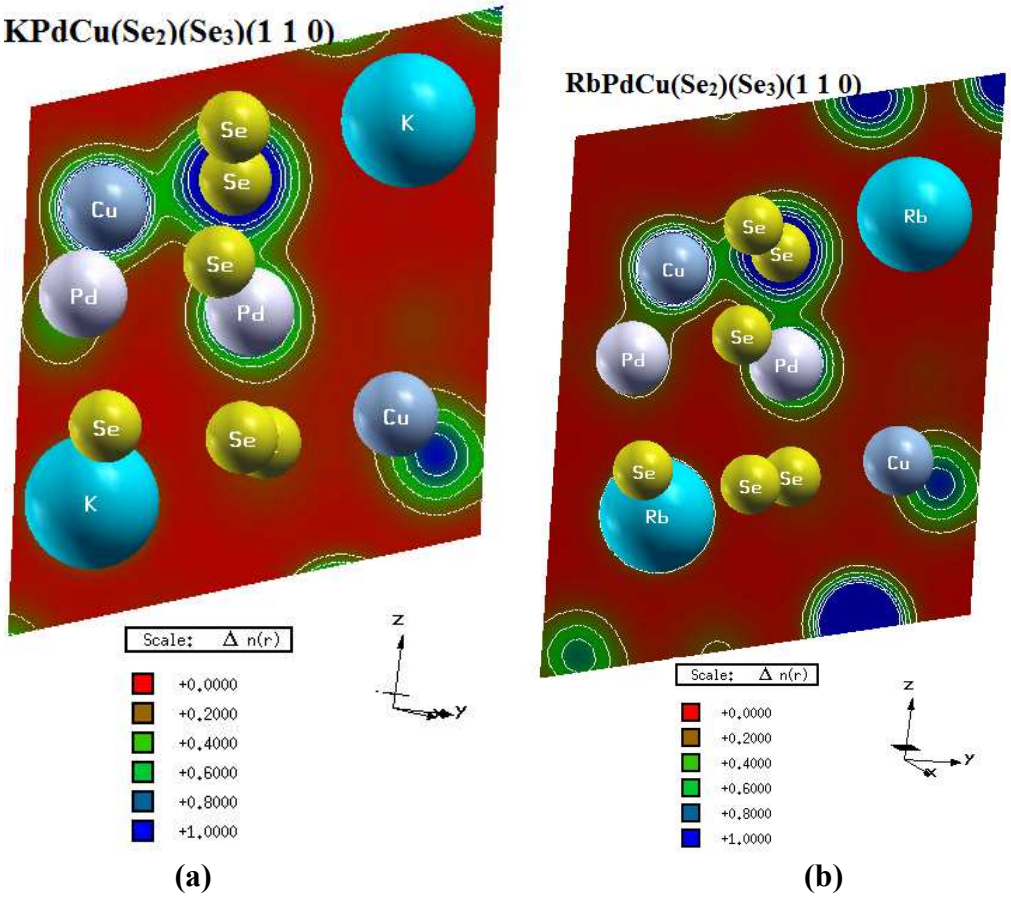
KPdCu(Se2)(Se3)(1 1 0)
Se
Se
K
Cu
Se
Pd
Pd
Se
Se
Cu
K
Scale: Δ n(r)
+0.0000
+0.2000
+0.4000
+0.6000
+0.8000
+1.0000
z
y
RbPdCu(Se2)(Se3)(1 1 0)
Rb
Se
Se
Cu
Se
Pd
Pd
Se
Se
Se
Cu
Rb
Scale: Δ n(r)
+0.0000
+0.2000
+0.4000
+0.6000
+0.8000
+1.0000
z
y

(a) **(b)**

Fig. 4

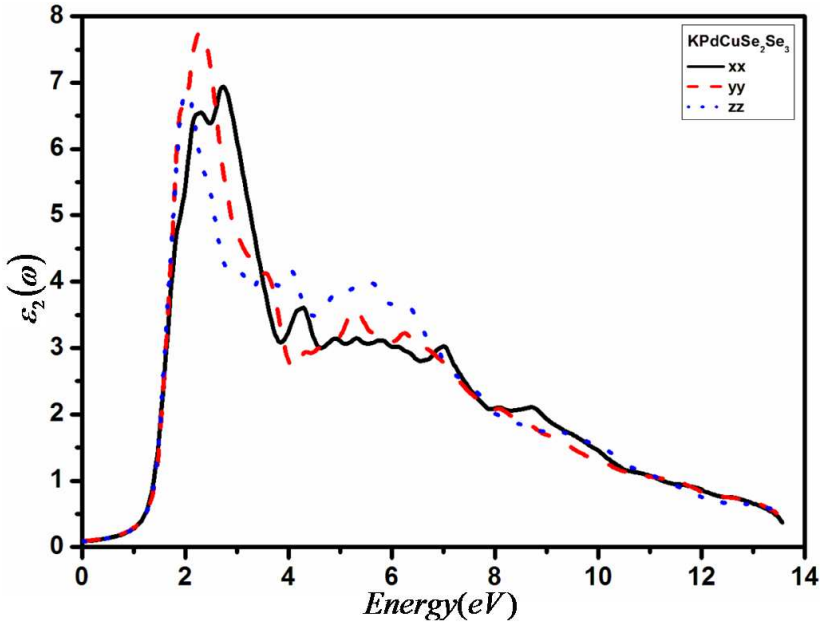
KPdCuSe2Se3
xx
yy
zz
ε2(ω)
Energy(eV)
0
1
2
3
4
5
6
7
8
0
2
4
6
8
10
12
14

(a)

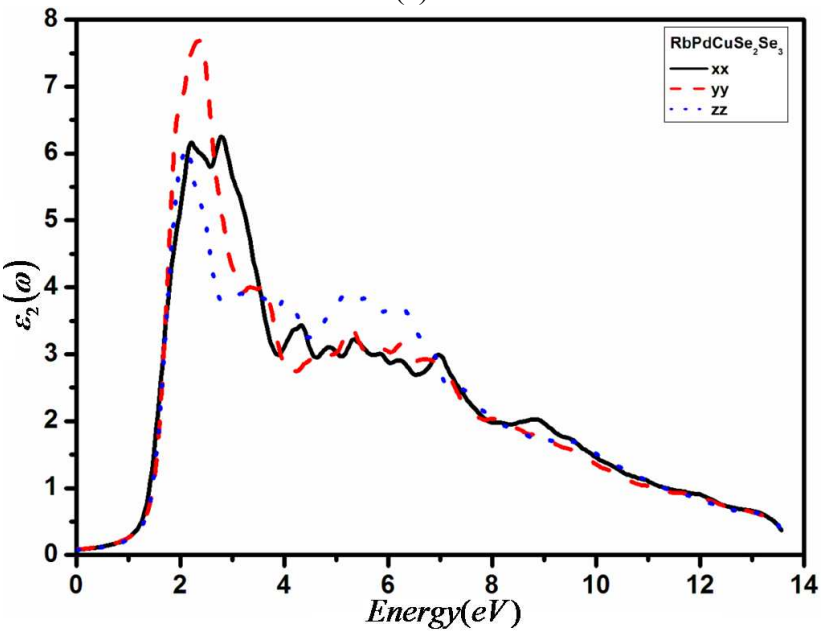
RbPdCuSe2Se3
xx
yy
zz
ε2(ω)
Energy(eV)
0
1
2
3
4
5
6
7
8
0
2
4
6
8
10
12
14

(b)

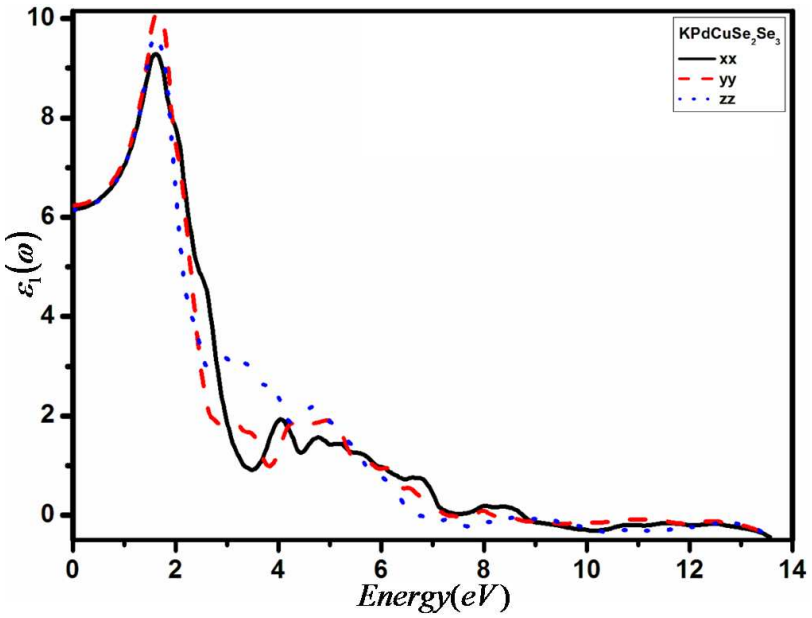
KPdCuSe2Se3
xx
yy
zz
ε1(ω)
Energy(eV)

(c)

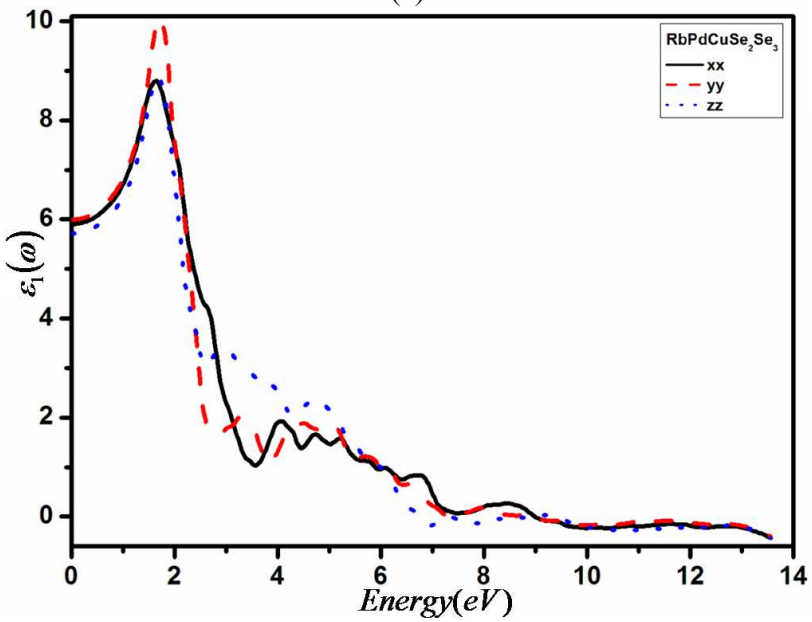
RbPdCuSe2Se3
xx
yy
zz
ε1(ω)
Energy(eV)

(d)

Fig. 5:

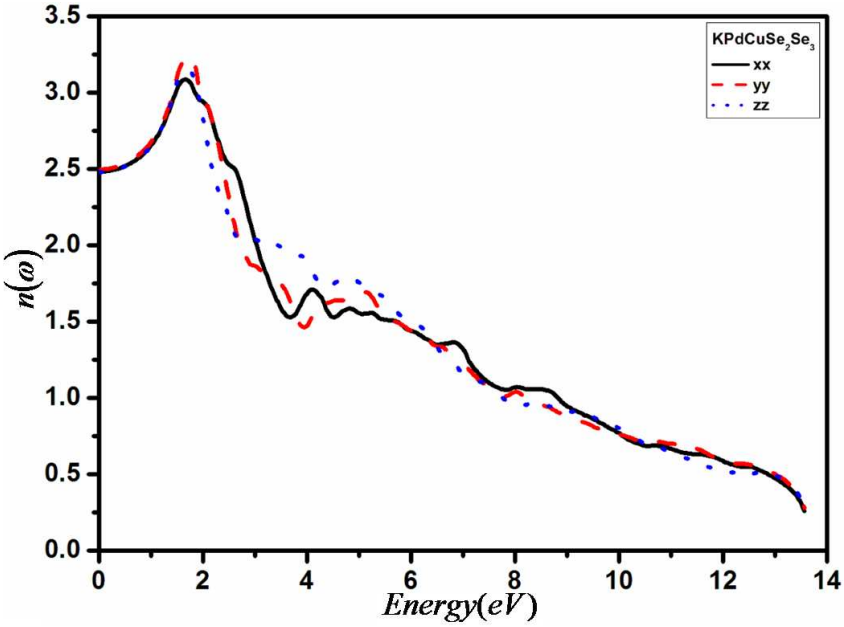
KPdCuSe2Se3
xx
yy
zz
n(ω)
Energy(eV)
0.0
0.5
1.0
1.5
2.0
2.5
3.0
3.5
0
2
4
6
8
10
12
14

(a)

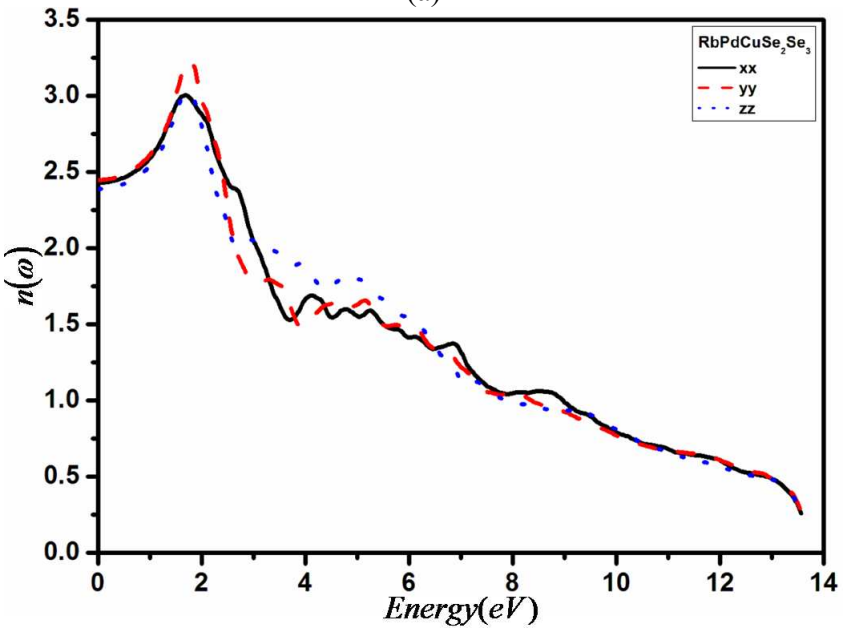
RbPdCuSe2Se3
xx
yy
zz
n(ω)
Energy(eV)
0.0
0.5
1.0
1.5
2.0
2.5
3.0
3.5
0
2
4
6
8
10
12
14

(b)

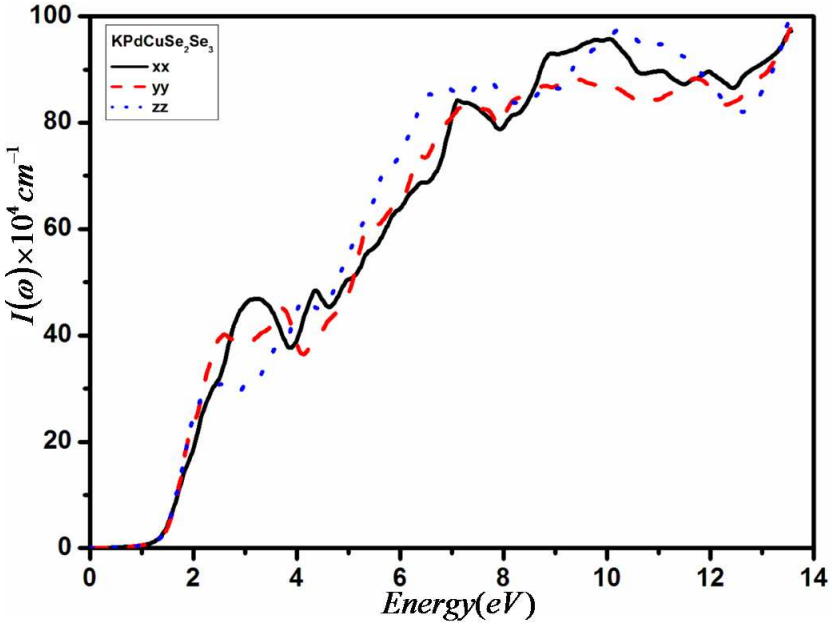
KPdCuSe2Se3
xx
yy
zz
I(ω)×10^4 cm^-1
Energy(eV)
0
20
40
60
80
100
0
2
4
6
8
10
12
14

(c)

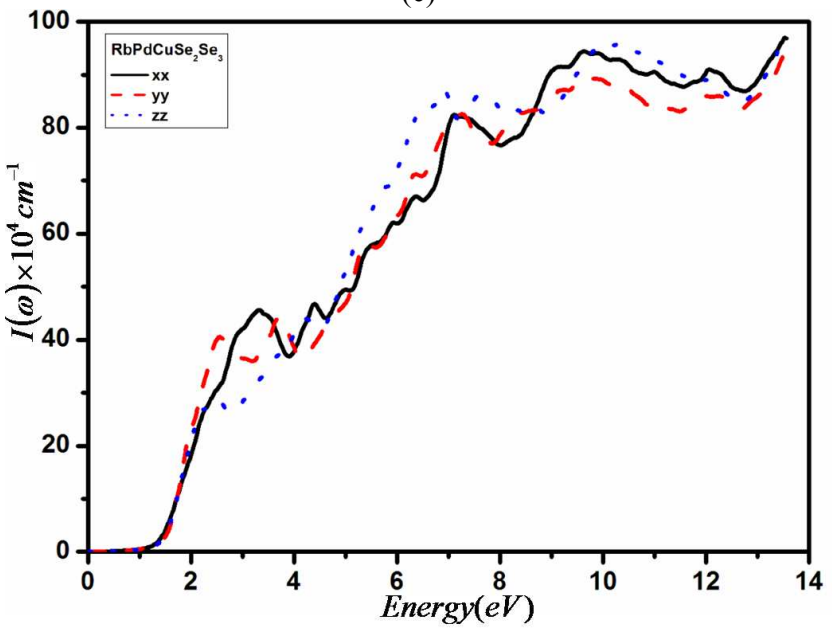
RbPdCuSe2Se3
xx
yy
zz
I(ω)×10^4 cm^-1
Energy(eV)
0
20
40
60
80
100
0
2
4
6
8
10
12
14

(d)

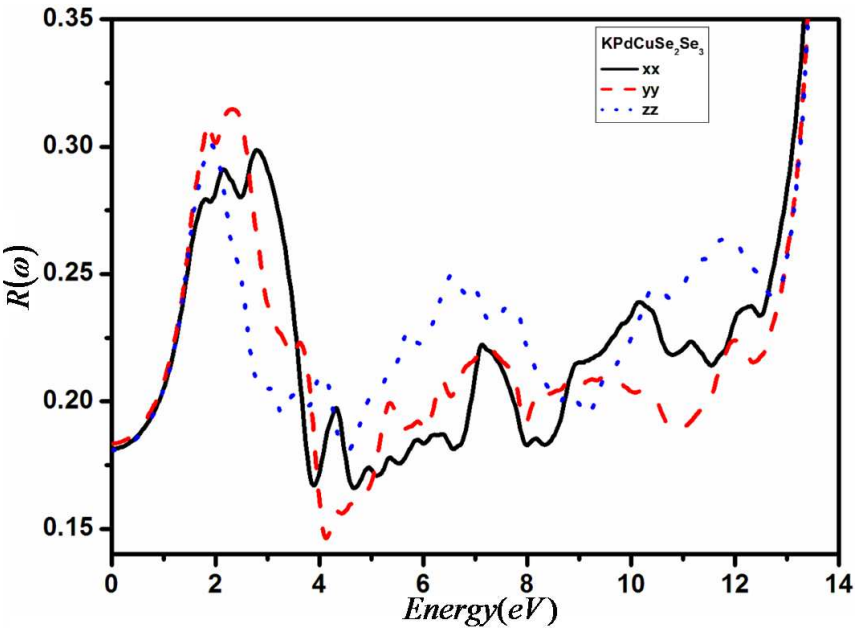
KPdCuSe2Se3
xx
yy
zz
R(ω)
Energy(eV)
0.35
0.30
0.25
0.20
0.15
0
2
4
6
8
10
12
14

(e)

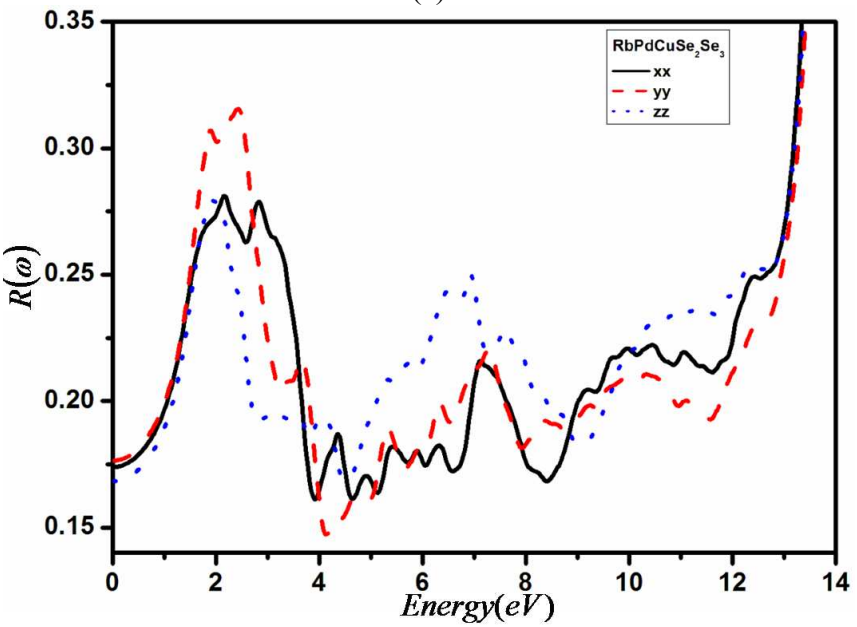
RbPdCuSe2Se3
xx
yy
zz
R(ω)
Energy(eV)
0.35
0.30
0.25
0.20
0.15
0
2
4
6
8
10
12
14

(f)

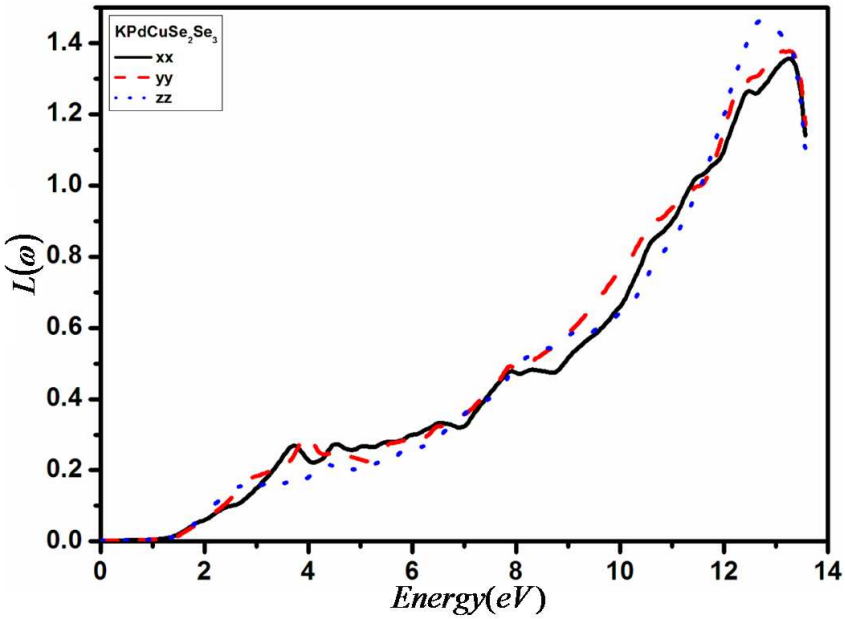
KPdCuSe2Se3
xx
yy
zz
L(ω)
Energy(eV)
0.0
0.2
0.4
0.6
0.8
1.0
1.2
1.4
0
2
4
6
8
10
12
14

(g)

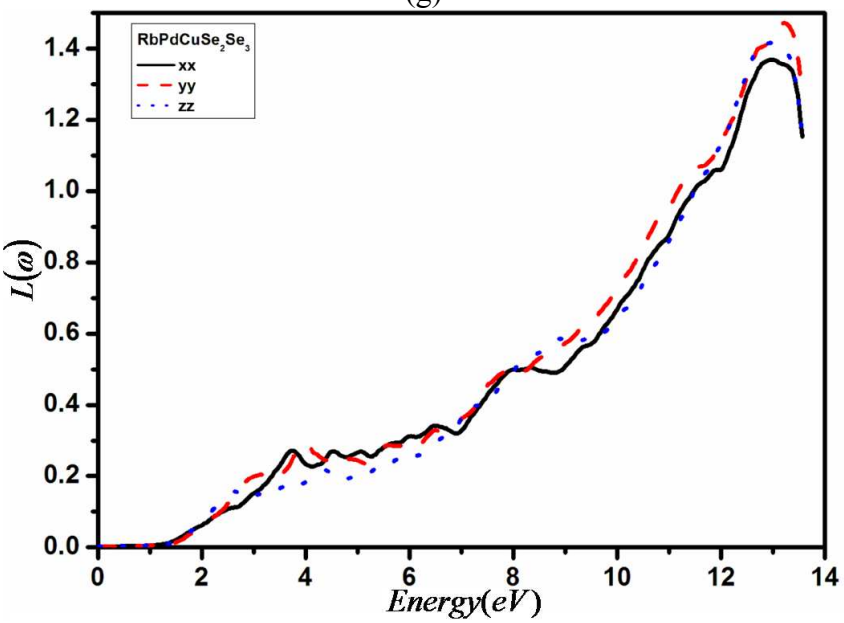
RbPdCuSe2Se3
xx
yy
zz
L(ω)
Energy(eV)
0.0
0.2
0.4
0.6
0.8
1.0
1.2
1.4
0
2
4
6
8
10
12
14

(h)

Fig. 6:

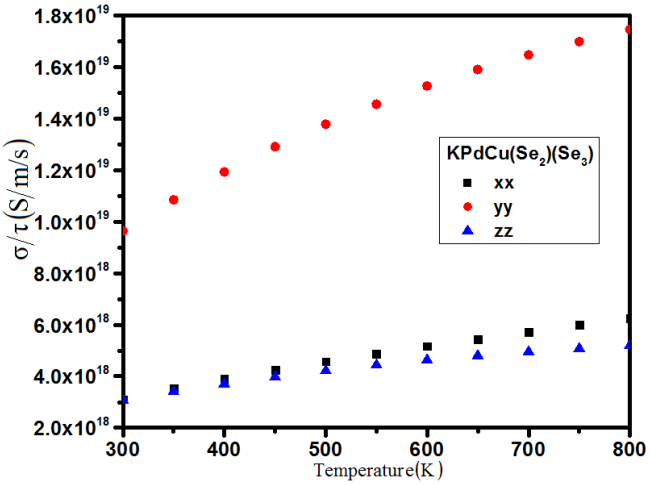
KPdCu(Se2)(Se3)
xx
yy
zz
σ/τ(S/m/s)
Temperature(K)

(a)

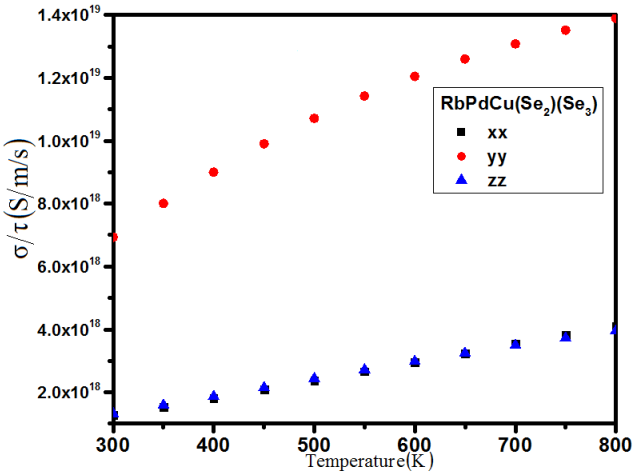
RbPdCu(Se2)(Se3)
xx
yy
zz
σ/τ(S/m/s)
Temperature(K)

(b)

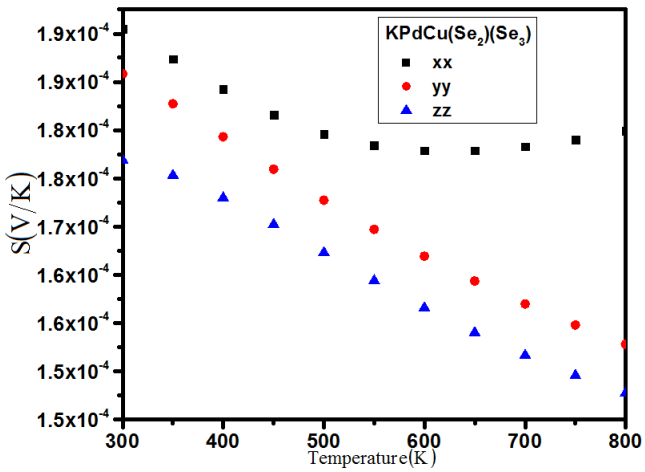
KPdCu(Se2)(Se3)
xx
yy
zz
S(V/K)
Temperature(K)

(c)

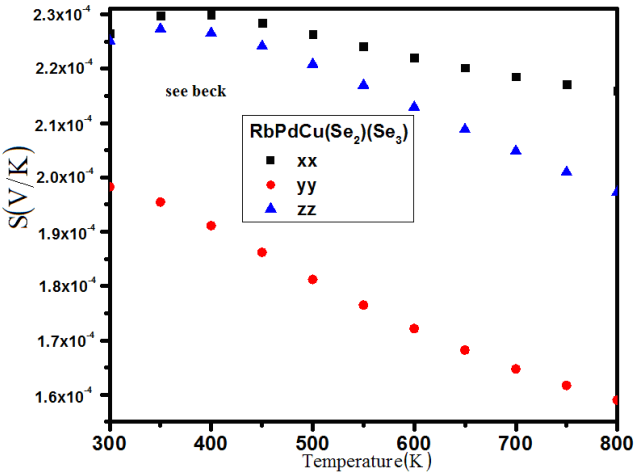
see beck
RbPdCu(Se2)(Se3)
xx
yy
zz
S(V/K)
Temperature(K)

(d)

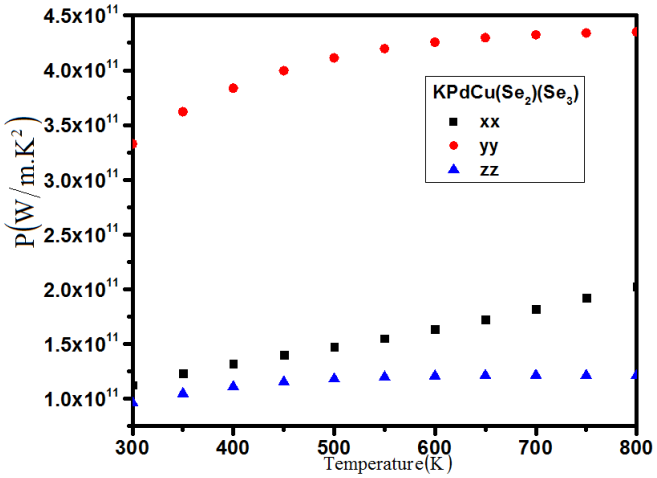
KPdCu(Se2)(Se3)
xx
yy
zz
P(W/m.K2)
Temperature(K)

(g)

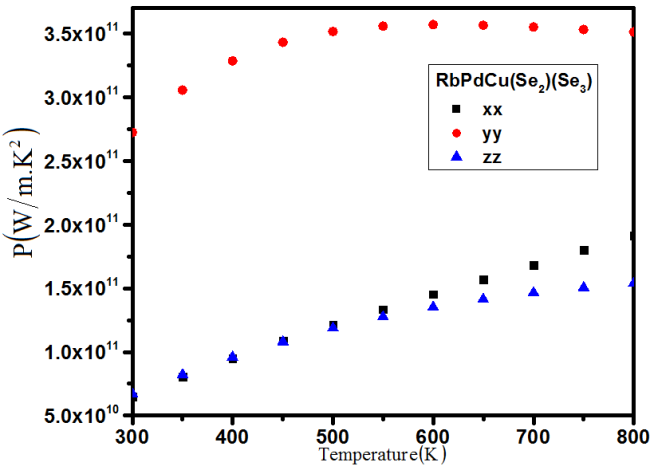
RbPdCu(Se2)(Se3)
xx
yy
zz
P(W/m.K2)
Temperature(K)

(h)

Fig. 7: